VERIFICATION OF MICROPHYSICAL RETRIEVALS FROM POLARIMETRIC RADAR

Peter T. May[1] and Thomas D. Keenan

Bureau of Meteorology Research Center,

Melbourne, Victoria, 3001, AUSTRALIA

Date: May 27, 2004

Submitted to Journal of Applied Meteorology

[1] Corresponding author address: Dr. P.T.May, BMRC, GPO Box 1289K, Melbourne, 3001, Vic. Australia; email: p.may@bom.gov.au

Abstract

Polarimetric radar data has been used to produce microphysical classifications. This type of analysis is run in an "operational" mode from several research radars including the G-Pol radar in Darwin. However, these classifications have had very little verification. The approach taken here is to use a combination of 50 MHz and 920 MHz wind profiler data to provide verification data for the radar pixels over the profiler. The retrievals of hail/rain mixtures is remarkably robust, however there are some issues regarding other microphysical classes. This includes difficulties in detecting melting snow layers in stratiform rain that is largely due to the re-sampling of the radar volume data onto a grid.

1. Introduction

A number of groups are presently using polarimetric radar measurements to automatically estimate the microphysical type of the hydrometeors within a radar volume (e.g. Vivekananandan et al, 2000; Straka et al, 2000; Keenan 2003). These applications hold a great deal of promise for both research and operational applications (e.g Shurr et al, 2003). The algorithms that underpin these systems exploit the fact that different hydrometeor species occupy different parts of the polarimetric variable phase space. However, these hyper-volumes have significant overlapping areas. Therefore, fuzzy-logic approaches have been used to determine the best estimate of the hydrometeor species.

These algorithms are now being applied routinely at several centres, e.g. at Colorado State University (CHILL radar), NCAR (S-Pol radar), NSSL (Nexrad upgrade project radars) and BMRC (C-Pol radar). These radars are all 10 cm wavelength systems except the latter (C-Pol, Keenan et al, 1998) which has a radar wavelength of 5.5 cm. These data are being supplied in real time for field programs and, in the case of G-POL, to the wider community through the US DOE ARM program (www.arm.gov) as an external data set associated with the Darwin site. As these data become available, a significant question concerns their reliability. Testing the separation between snow and rain is relatively straight-forward in the USA and good success has been found (e.g. Schurr et al, 2003). However, hail and graupel are much harder to verify. Ground surveys of large hail are notoriously difficult and most efforts at verifying the polarimetric retrievals have

effectively concluded that "the retrievals look reasonable". There are occasionally fortuitous observations that lend support to the retrievals. Fig. 1 shows a RHI cross-section through a very deep, intense thunderstorm over the Tiwi Islands north of Darwin. The top panel shows the reflectivity. Note that there is a distinct flare echo extending behind the storm radially from an altitude of 4-5 km. Such flare echoes arise from multiple scattering of the radio waves and are an indicator of large, wet hail (Wilson and Reum, 1988). The lower panel shows the corresponding microphysical classification and an extensive rain/hail mixture region is seen in front of the flare. Such observations are consistent, but cannot be relied on for more systematic analysis as they are fairly rare.

There has been substantial work over the past few years using wind profiler and polarimetric radar data that have demonstrated that significant hail is often present in tropical convective showers (May et al, 2001, 2002). Although hail at the surface is rare in the tropics, the profilers at Darwin can be used to identify hail aloft. Furthermore, convection in Darwin is so frequent, that a reasonable number of cases are easily collected even though the use of profiler data means we are limited to verifying the data in a single column.

This paper will seek to verify the accuracy and limitations associated with the C-Pol retrievals in Darwin using profiler data as well as examining the robustness of the fuzzy logic retrievals themselves. The profiler comparisons will focus on hail detection and some insights into storm dynamics and the interpretation of profiler spectra will be discussed. The latter part of this work will utilise the regular RHI scans that are

performed along a cross-section over the wind profiler site to look at melting snow signatures and limitations of the approach being utilised for the classifications in stratiform rain.

The observing network in Darwin has recently been upgraded with the addition of an ARM (Atmospheric Radiation Measurement) program suite of instrumentation. The total observing system is probably the most complete in the tropics. In particular the BMRC C-Pol (C-band Polarimetric) radar (Keenan et al, 1998) is located approximately 23 km from the 2 wind profilers, one operating at 50 MHz and the other a 920 MHz,. These systems operate routinely and data from them is available through the ARM external data archive. Two sets of C-Pol data are available from the ARM archive. These are Cartesian grids of reflectivity and microphysical classification of the detected hydrometeors. These classifications look "reasonable", but until now are essentially un-verified. This paper examines some examples of these data and uses the profiler data to provide some ground truth for the microphysical classifications of the radar.

2. C-Pol radar and hydrometeor classification

The C-Pol radar runs a "volume scan" once very 10 minutes. These scans consist of a series of conical sweeps at a sequence of increasing elevations. Data is sampled every 300 m out to a range of 150 km. This builds up a three dimensional picture of cloud systems. Note that at 150 km the minimum detectable signal with the radar is about 0 dBZ, so the radar does see substantial amounts of non-precipitating cloud although

clearly much less than cloud radars. The volume scan data is then interpolated onto a Cartesian grid with a horizontal resolution of 3 km and a vertical resolution of 500m and a "fuzzy classification" performed. This may seem like a coarse horizontal resolution, but given the data are collected over a 10 minute volume, the spatial sampling is fairly consistent with the expected movement of a cell during the 10 minute data acquisition. An RHI scan is then performed at an azimuth pointing over the wind profiler site to provide high vertical resolution data.

The polarimetric radar alternates between horizontal and vertical polarization on a pulse to pulse basis. Thus, in addition to reflectivity, there are a number of additional parameters available. These include the difference in reflectivity between the signals at the two polarization which is represented as the ratio Z_H/Z_V (Z_{DR}), the correlation between the signals at the two polarizations, the D_{HV} (0), and the rate of change of the differential phase on propagation, the K_{DP}. The Z_{DR} is a measure of the mean oblateness of the hydrometeors. For example large drops are oblate and produce large values of Z_{DR} (> 3 dB) whereas snow and large hail tumbles and have no preferred orientation so that the Z_{DR} is typically near 0 dB. The D_{HV} (0) is near 1 for most rain, but drops substantially if the drops are very large (Mie scatter effects become important) or if there is mixed phase precipitation. The K_{DP} can be understood by considering that the two polarizations essentially see different water paths because of the oblateness of rain drops and therefore one polarisation is retarded relative to the other (as the refractive index is > 1). In general different hydrometeors occupy different parts of the 4 dimensional phase space so that estimates of hydrometeor type can be obtained from the radar The

hydrometeor species are given in Table 1. These are not completely un-ambiguous and a fuzzy logic approach is used to combine the polarimetric estimators. Some environmental information is also used. This approach is described in detail by Straka et al (2000) and Keenan (2003).

Following the above general principles, the classification procedure is based on the use of fuzzy logic membership functions with a four step process employed to define hydrometeor species (j=1-10). The fours steps are:-

1. *The probability (P^T_j) of each hydrometeor species being present is derived based on the environmental temperature of the radar sample volume,*

$$P_j^T = P_j(T_j^{lower}, T_j^{upper}, T) \qquad (6)$$

where $P_j(T_j^{lower}, T_j^{upper}, T)$ is the temperature membership function, T is the temperature of the sample volume, and T_j^{lower} and T_j^{upper} represent temperature bounds from Table 1 considered consistent with the physical existence of the various hydrometeor species.

2. *The probability (P^R_j) of each species is deduced based on the polarimetric variables R_k (where k=1, 4 corresponds to Z_{HH}, Z_{DR}, K_{DP} and $D_{HV}(0)$)using the ranges provided in Table 1*

$$P_j^R = \sum_k W_k P_j^k (R_k^{lower}, R_k^{upper}, R_k) / \sum_k W_k \qquad (7)$$

where W_k is a weighting function for each polarimetric variable (all equal to one in this case).

3. *The above two probabilities are then combined to estimate P_j the aggregated or total probability of each species,*

$$P_j = P_j^T + P_j^R \tag{8}$$

4. *If the maximum P_j meets the following criterion*

$$\left|\max(P_j) - \overline{P}\right| \geq 1.75 s_p \tag{9}$$

where F_P is the standard deviation of the hydrometeor class probabilities, class j is assigned. Hence missing classification values are evident in low confidence situations.

A Gaussian Bell function structured with 5% percentile tails is employed for assigning class membership probabilities. The choice of the Gaussian Bell classification function was somewhat arbitrary. It is interesting to consider how strongly these classifications are defined. The fuzzy process produces an estimate of weight for each of the microphysical classification types and the strongest is selected. The ratio of the weights of the second most likely to the most likely is often quite large, ~ 0.8 (if it was 1 there would be no difference, if it was 0 then we can be very confident in the

classification). Plots of time height cross-sections of the ratio of weights (not shown) indicate that even where rain is not detected in the region below the freezing level, it is still a strong possibility. When rain is the most likely, it is often, but not always, strongly selected. Likewise, snow tends to have a large weight above the freezing level even if it was not the most likely candidate. Given this observation, it is somewhat surprising that the classifications themselves are not more noisy. In fact they seem internally robust despite the often high second weights. The fuzzy logic classification procedure is undertaken either on a gate by gate basis in radial radar space (for RHI scans) or on a Cartesian grid (for volume scans).

An example of the radar data and the microphysical classification is shown in Fig. 1. This figure nicely shows the presence of mixed phase (mainly wet graupel and rain hail mixtures) in the high reflectivity areas of a thunderstorm over the Tiwi islands north of Darwin. This is consistent with the very strong updrafts in these storms and their high level of electrical activity.

In general the microphysical classifications of the radar seem very reasonable (Straka et al, 2000; Vivekanandan et al 2000; Keenan 2003). However, they have not been independently verified. The remainder of this paper deals with using profilers to verify the polarimetric classification and to point out some problem areas.

3. Profiler studies of precipitation

Wind profilers have been used for the study of precipitation for more than a decade. The ability of the profilers to simultaneously observe spectral peaks associated with the clear air vertical motion and peaks associated with hydrometeors has allowed the estimation of rain drop size distributions (e.g. Wakasugi et al., 1986), snow size distributions (Rajopadhyaya et al , 1994) and studies of the radar bright-band (Drummond et al, 1996). More recently May et al (2001, 2002) examined several storms where there was significant production of hail and graupel with a combination of wind profiler and the G-Pol data. In particular, the combination of 50 MHz and 920 MHz profilers was used to directly sense particles with fall speeds greater than the asymptotic limit for rain drops. The 50 MHz Doppler spectra are usually dominated by the clear air echo peaks that are always seen, while the 920 MHz Doppler spectrum is dominated by returns from precipitation. A particularly clear example of this is shown in Fig. 2. Here the 920 MHz Doppler spectrum clearly shows a distinct double peaked structure. One peak corresponds to fall speeds of about 8 ms^{-1}, which is typical of rain as the D^6 dependence weights the spectra to large rain drops. The second peak, at fall speeds of about 13 ms^{-1}, is only explained by 1-2 cm sized hail. Note that the particles associated with the hail peak are ~ 10 times the diameter of those in the rain peak. These peaks have a similar amplitude, so that there are ~ 10^6 times as many drops in the rain peak as hail particles and 1000 times the water volume in the rain peak. This illustrates the ability of the profiler to differentiate even small concentrations of wet hail. Most cases are not this clear, but both rain and hail size can be measured from the profiler data (May et al, 2002).

It should also be remembered that the profiler vertical velocity spectra observations are taken over a period of 45 s out of a 1 minute cycle, so that there may be considerable variability of the vertical motion during the data acquisition. The importance of this will be clear in section 5.

One of the key tests of the C-POL classification will be the delineation of areas of mixed phase precipitation, in particular wet graupel and rain/hail mixtures. This is manifested in the profiler data as areas where there are significant signals in the profiler Doppler spectra corresponding to particle fall speeds greater than the asymptotic fall speed for rain (~$9.8/D^{0.4}$ ms^{-1} where D is the air density). This spectral information allows both the detction of hail larger than about 1 cm and some size information. Note that the un-ambiguous detection of graupel and small hail with profiler data alone is not possible as the fall speeds are similar to that of rain.

Thus, the details of the profiler Doppler spectra and the retrievals of microphysical characteristics can clearly be used to validate the C-Pol estimates.

4. Data sets

Data from several storms passing over the profiler have been examined for hail. These include cases of isolated single cell storms, continental squall lines and monsoonal storm complexes. This ensures that a range of storm intensities (as defined by maximum

vertical velocities) and different degrees of organization have been sampled. These cases include samples where hail was not detected in the profiler data or only weak hail signatures were present, as well as clear hail cases. Several of the cases also had distinct trailing stratiform regions and data collected from these regions were used to provide information for pure rain situations as well as to examine the difficulties of the grid based retrievals for retrieving thin layers of melting snow. High vertical resolution data from RHI scans were used for this purpose.

5. Verification: A case study

Fig 3 shows an example of a time height cross-section of the profiler reflectivity, vertical motion and reflectivity weighted fall speed relative to the air (i.e. the vertical motion measured with the 50 MHz profiler has been subtracted from the fall speed measured with the 920 MHz profiler) through a squall line. This example shows a strong updraft on the periphery of the main precipitation core. However, this updraft is within the cloud as demonstrated by a weak increase in the 920 MHz reflectivity (not shown). The maximum updrafts exceed 10 ms^{-1} and it is reasonable to expect that super-cooled drops are being lofted and significant riming and potential hail production is occurring. This is corroborated by the large fall speeds seen in the downdraft in the high precipitation area. The reflectivity weighted fall speeds exceeded 10 ms^{-1}, which is a strong indicator that hail is present.

One intriguing feature is the apparent upward moving precipitation next to the top of the main updraft. This is a feature that is often seen near the top of the leading edge of convection in profiler fall speed data. Detailed examination of the radar Doppler spectra shows that there are two peaks in the 50 MHz spectrum at these altitudes. The lower speed one is a downdraft and is the larger, but there is also a secondary upward peak and the 920 MHz spectral peak corresponds to this. What appears to be happening is there is some overturning during the 45 s data acquisition. This is also indicated in the reflectivity structure with the filamentary reflectivity structure overlaying the "upward" rain. The interpretation of this is the upward peak, which was probably present for only part of the 45 s record, was lofting rain and ice aloft. These were presumably small with small fall speeds so that both the 50 MHz and 920 MHz profilers see upward motion for part of the record. However, for most of the record there was a downdraft present as indicated by the stronger 50 MHz peak. Presumably, the precipitation in the downdraft, if there was any present, was evaporated, perhaps intensifying the downdraft, but there are no detectable echoes for the 920 MHz profiler during this part of the 45 s record. Thus the profiler apparently sees upward moving precipitation since the mean motion (weighted by the 50 MHz clear air reflectivity) was downward while the precipitation echo was in the updraft portion of the record. There is also an interesting "step" in the hight of the brightband at about 1150 UTC which is reflected in the height of the freezing level in soundings taken before and after the storm.

There is also an indirect confirmation of mixed phase and graupel production in the area. Lightning echoes are seen in the profiler data. These are visible as spots of very high

reflectivity and spectral width and anomalous (meaningless) apparent vertical motions. These are most clearly seen in the 50 MHz data but are also visible as small bright spots in the 920 MHz reflectivity at altitudes ~ 7-8 km just after the main peak of precipitation. This is not the radar seeing the direct radio emission from the lightning as that would appear at random height, but rather is radar reflections off the ionization trail of the lightning as it is advected through the radar beam. There is also the possibility that they are being detected through sidelobes, but this is argued against by their height distribution with the most common detections just above the freezing level and near storm top and by the fact that the echoes appear in both of the profilers at the same height (the profilers have very different side-lobes). These lightning echoes typically have very large spectral widths (covering the entire Nyquist interval so the full width is unknown) and very high power at 50 MHz completely masking the clear air and precipitation spectral peaks. Such lightning echoes have been recorded in the literature (e.g. Larsen and Rottger, 1987) and were discussed in detail by Atlas and Williams (2003). Atlas and Williams discussed the frequency dependence where they saw the lightning echoes with a 915 MHz profiler, but not with a 10 GHz profiler. These results illustrate that this can be extended to very intense echoes at 50 MHz.

Fig 4 shows the corresponding time height cross-section of the C-Pol gridded reflectivity and microphysical classification data over the profiler site. This has 10 minute time resolution so is of course much blockier than the profiler time series. The time height cross-section of the C-pol data above the profiler is broadly consistent with the profiler data in the convective region, the transition and stratiform regions of the squall line.

There is a substantial region where the microphysical classification is wet graupel and rain/hail mixtures and this region corresponds very closely with the profiler regions of high fall speed and the areas of snow and rain appear consistent with conceptual models of such systems.

However, the C-Pol classifications are far from perfect. This is most in evidence in the stratiform part of the squall line (1030-1200 UTC). There is a substantial area where there is a wet graupel classification above the melting level. This is in the region where the temperature is between –10 and 0°C and that aggregation of the snow crystals is likely to be occurring. While this is a mis-classification, it does point to the microphysical data being useful in identifying significant physical processes in the precipitation. However, it will be shown that this is at least partly induced by a lack of spatial resolution in the data.

Another problem area is the lack of a melting snow layer in the stratiform region. The only pixels where this occurs is in the small region where the gridded reflectivity shows a distinct bright-band signature. The bright-band is obviously much clearer in the profiler data, but the interpolation procedure used for the C-Pol data washes out this signature. This has been further examined by an examination of RHI data. The C-Pol radar performs an RHI scan directed over the profiler site at the end of every volume scan. The classifications for the RHI is done on a raw pixel level and it is seen in Fig 5 that the brightband is well resolved and a narrow layer of melting snow comes up in the classification. Conversely, the aggregation signature of anomalous wet graupel noted in

the previous paragraph is partially lost. An active convective element with a rain-hail mixture as well as a large area of wet graupel around the cell core is also evident. Thus the melting snow classifications where there is very good horizontal and vertical resolution appears fairly robust. In order to test if the problem was associated with the grid resolution, the volume data was re-sampled onto 0.5, 1, 1.5 and 2 km horizontal resolution grids. However, the problems that were seen in the original grids remain, although the sampling did produce changes in the detailed reflectivity and classification structure. Thus the prime problem is in the limited spatial sampling in elevation inherent in volume data.

Another feature in the classification cross-section is the noisiness of the region with high and low density snow and dry graupel above the wet graupel in Fig. 4. This is an indication that the different hydrometeor classifications are not well separated in their phase space and that the classifications of these types is uncertain. This problem is also made worse by the poor resolution and smearing inherent in the gridding of the data, as there appears to be much less noise in the snow/dry graupel classifications in the RHI data (Fig. 5). However, in this case almost no high density snow is seen even around the graupel areas. One recommendation arising from this is to combine the high and low density snow classifications into a single snow classification.

6. Lightning echoes as verification data

As noted above the profilers are able to sense echoes from lightning ionisationation channels. Fig. 6 shows the location of lightning detections based on the occurrence of the very broad spectra seen in the 50 MHz data overlaid on the C-Pol profiles above the profiler location (as before). This shows very nicely the occurrence of the lightning behind the initial updraft indicating the need for some time to develop a charged mixed phase region. It also shows the concentration of lightning detections in the layer just above the freezing level (~ 4.9 km) and near the storm top. The upper layer descends with the storm echo top.

These data are consistent with charging models of lightning production with charge separation occurring where there is a mixture of graupel and ice crystals between 0 and -20°C leading to large gradients in charge and near the storm top as well as analyses combining lightning detection and radar data (Williams, 1989). Furthermore they give credence to the classification of rain/hail mixtures and wet graupel in the region of the lightning occurrence. These signatures are much weaker in oceanic convection (to be discussed next) when there is little lightning activity (Williams et al., 1992).

7. Systematic verification of the classifications

The previous sections have discussed some case studies illustrating the qualitative consistency between the profiler observations and the polarimetric classifications. In

order to put this onto a more quantitative basis, the profiler data was sorted into time-height cross-sections of the reflectivity from the rain and hail components separately and then mapped onto the polarimetric sampling. That is, a profiler hail detection was flagged if significant "hail" was seen at a given height range during the first 6 minutes of the ten minute volume scan. This was to allow for the scanning time and the spatial averaging inherent in the volume estimate. This procedure has been performed and columns of detections compared for 6 cases totalling over 10 hours of precipitation over the profiler. Two of these were cases from monsoonal convection where the vertical motions were expected to be much weaker, although one (February 17, 2003) had a clear hail signature in both data sets. This was to provide a test for the non-occurrence of the hail signatures in convection with high rainfall rates, but weak vertical motions and little hail expected to develop. In these monsoon cases little or no hail signatures were seen in either data set.

An event was classed as a detection if there was a hail signature present in the column for a given 10 minute interval within the 6 time series. The results are summarised in Table 2. Objectively, there were 8 hits, 2 misses and 2 false alarms in over 10 hours of data where precipitation was over the profiler. Of the two misses, one sample only had hail in the small part of the 10 minute cycle and this was adjacent to a clear hit. The second miss had only a weak signature in the profiler data with relatively low reflectivity. This may be a false detection by the profiler. Of the false alarms, one was only a single pixel in a relatively low reflectivity time-height cross-section while the other was adjacent to a very strong detection. Although tagged as a false alarm it is quite likely that there was

hail present in the 3km by 3 km volume and the "false alarm is a product of the spatial sampling of the C-Pol data.

8 Conclusions

Several cases of convective storms have been examined using the combination of the wind profiler and polarimetric radar data. Of these several highlight the large over-turning and entrainment at the top of the leading edge of convection in the profiler data including the case examined in detail in this paper. The profiler data is clearly useful in verifying the C-Pol microphysical classifications. Furthermore the classifications of rain/hail mixtures themselves are remarkably robust. The number of false alarms and missed detections were very low considering the limited data available, the fact that gridded data was used and the limited separation in the measurement phase space of different hydrometeor combinations.

One area of concern in the basic methodology is the attempt to define too many closely separated classifications. This is seen clearly in Figs 4 and 5. These figures indicate that the high and low density snow classifications should be combined into a single snow classification.

The gridded classification problem does have some problems. This is particularly evident in stratiform rain with a brightband where the radar signatures are smeared in the gridding process. This results in two problems. One is an apparent layer of wet graupel

above the melting level that appears erroneous but may be related to aggregation of the ice crystals and the other is the lack of detection of melting snow. These problems may be alleviated by applying the classification to the raw data and then gridding the classifications or by using the full three or four dimensional information available to refine and edit the classification fields. The former faces some problems on how to perform the interpolation of the classifications onto a grid.

The C-pol data set will be very useful in placing the ARM cloud data in context with respect to the cloud origin and the characteristics of the parent convection. These gridded data are being made available as an external data set to the ARM community as is the profiler data. (www.arm.gov).

Acknowledgment

This work is partly supported by the US Department of Energy Atmospheric Radiation Measurement (ARM) program.

References

Atlas, D. and C.R. Williams, 2003, Radar echoes from lightning and their microphysical environment, Geophys. Res. Lett., **30**, 66-1 - 66-4, doi:10.1029/2002GL016521

Drummond, F. J., R.R. Rogers, S.A. Cohn, W.L. Ecklund, D.A. Carter, J.S. Wilson, 1996: A New Look at the Melting Layer**,** *J. Atmos. Sci.*, **53**, 759–769

Keenan, T.D., 2003: Hydrometeor classification with a C-band polarimetric radar, *Aust. Meteor. Mag.*, **52**, 23-31

Keenan, T.D., K. Glasson, F. Cummings, T.S. Bird, J. Keeler and J. Lutz, 1998: The BMRC/NCAR C-Band polarimetric (C-POL) radar system., *J. Atmos. Oceanic Tech.*, **15**, 871-886.

Larsen, M.F., and J. Röttger, 1987: Observations of Thunderstorm Reflectivities and Doppler Velocities Measured at VHF and UHF**.**, *J. Atmos. Oceanic Tech*., **4**, 151–159.

May, P.T., A.R. Jameson, T.D. Keenan and P.E. Johnston, 2001, A comparison between polarimetric radar and wind profiler observations of precipitation in tropical showers, J. Appl.Meteor., **40**, 1702-1717.

May, P.T., A. R. Jameson, T.D. Keenan, P.E. Johnston and C. Lucas, 2002: Combined wind profiler/polarimetric radar studies of the vertical motion and microphysical characteristics of tropical sea breeze thunderstorms, *Mon. Wea. Rev*., **130**, 2228-2239.

Rajopadhyaya D.K., P.T. May and R.A. Vincent, 1994, Retrievals of ice particle size distributions from VHF wind profiler Doppler spectra, J. Atmos. Oceanic Tech., **11**,1559-1568

Schuur, T., A. Ryzhkov, P. Heinselman, D. Zrnic, D. Burgess, and K. Scharfenberg, 2003: Observations and classification of echoes with the polarimetric WSR-88D radar, NSSL report, October, 2003, 46 pp.

Straka, J.M., D. Zrnic and A. Ryzhkov, 2000: Bulk hydrometeor classification and quantification using polarimetric radar data: Synthesis of relations. *J. Appl. Meteor*., **39**, 1341-1372.

Wakasugi, K., A. Mizutani, M. Matsuo, S. Fukao and S. Kato, 1986: A direct method for deriving drop-size distribution and vertical air velocities from VHF Doppler radar spectra, *J. Atmos. Oceanic Tech.*, **3**, 623-629.

Williams, E.R., 1989: The tripole structure of thunderstorms, *J. Geophys. Res*., **94**, 13151-13167.

Williams, E. R., S.A. Rutledge, S. G. Geotis, N. Renno, E. Rasmussen, E. and T. Rickenbach, 1992: A radar and electrical study of tropical “Hot Towers”. *J. Atmos. Sci.*,. **49**, 1386–1396.

Wilson, J.W., and D. Reum. 1988: The Flare Echo: Reflectivity and velocity signature**.** *J. Atmos. Oceanic Tech.*. **5**,. 197–205.

Vivekanandan, J., D.S. Zrnic, S.M. Ellis, R. Oye, A.V. Ryzhkov and J. Straka, 2000: Cloud Microphysics Retrieval Using S-Band Dual-Polarization Radar Measurements., Bull. Amer. Meteor. Soc., 80, 381-388.

Table Captions

Table 1 Ranges of polarimetric variables and temperature for various hydrometeor species.

Table 2. Summary of hail detections over 6 cases

Figure Captions

Figure 1 RHI cross-section of a thunderstorm over the Tiwi Islands north of Darwin. Note the flare echo extending behind the cell coinciding with the detection of a rain hail mixture.

Figure 2 Doppler spectra collected with the 50 Mhz profiler (solid) and 920 MHz profiler (dotted) at Darwin. The asymptotic limit for rain fall speeds relative to the mean air motion ($w \sim 5ms^{-1}$) seen by the 50 MHz profiler is also included. The high fall speed peak corresponds to hail while the other is rain (After May et al., 2001)

Figure 3 Time height cross-sections of the reflectivity measured with the 920 MHz profiler between 1000 and 1230 UTC on November 4, 2001 (top), mean vertical motion measured with the 50 MHz profiler with an overlaid contour of zero vertical motion (middle) and the reflectivity weighted precipitation fall speed estimated by the difference

between the Doppler velocity measured with the 920 MHz profiler and the vertical motion subtracted. The contours of the lower panel are at fall speeds of -2 and -10 ms^{-1}.

Figure 4 Time height cross-section of the C-Pol measurements of reflectivity on the grid point closest to the wind profiler location between 1000 and 1230 UTC on November 4, 2001 (top) and the corresponding microphysical classification. These data are on 2.5 by 2.5 km grids with a vertical sampling of 500m. The actual beam heights that were used in creating these data are marked by the horizontal lines on the left of the top panel.. Contours of reflectivity are overlaid on this figure.

Figure 5 RHI scan at 1119 UTC on November 4, 2001 showing the reflectivity (top) and classification (bottom) . This shows an active convective element with a rain-hail mixture as well as a large area of wet graupel around the cell core. Of particular interest here is the narrow layer of melting snow that is resolved in the stratiform region farther from the radar. Contours of radar reflectivity are overlaid on these panels.

Figure 6 Another time height cross-section of the reflectivity and classifications for 0500 to 1000 UTC on December 10, 2002. However, in this case the location of lightning echoes in the profiler data have been overlayed (dark lines) along with contours of reflectivity as before. This was a very electrically active case although the most intense convection missed the profiler. However, an extensive region of wet graupel is visible prior to and in the electrically active period.

Table 1 Ranges of polarimetric variables and temperature for various hydrometeor species.

	Z_{HH} (dBZ)	Z_{DR} (dB)	$D_{HV}(0)$	K_{DP} (deg km^{-1})	Temperature (^{o}C)
Drizzle	10-25	0.2 to 0.7	>0.97	0 to 0.06	>-10
Rain	25 to 60	0.5 to 4	>0.95	0 to 20	>-10
Snow (Dry,low density)	-10 to 35	-0.5 to 0.5	>0.95	-1 to 1	< 0
Snow[2] (Dry, High density)	-10 to 35	0.0 to 1	>0.95	0 to 0.4	<0
Snow (Wet, melting)	20 to 45	0.5 to 3	0.5 to 0.9	0 to 1	0 to 5
Graupel, dry	20 to 35	-0.5 to 1	>0.95	0 to 1	<0
Graupel, wet	30 to 50	-0.5 to 2	>0.95	0 to 3	-15 to 5
Hail, small < 2cm wet	50 to 60	-0.5 to 0.5	0.92 to 0.95	-1 to 1	-15 to 5
Hail, large > 2 cm wet	55 to 65	-1 to 0.5	0.90 to 0.92	-1 to 2	-25 to 5
Rain & Hail	45 to 80	-1 to 6	>0.9	0 to 20	-10 to 10

[2] Rimed and aggregated snow.

Table 2. Summary of hail detections over 6 cases

Date	Time of C-Pol detection	comment	Time of profiler detection	comment
4/11/01	1030		1030	
	1040			False alarm because of spatial averaging?
17/11/01			0930	Leading edge midway thru' 10 minures
	0940		0940	
10/2/02	0550		0550	
			0600	Low Z, scattered in height
5/2/03	0450		0450	
	0500	Weak, scattered in height	0500	Weak, scattered in height
16/2/03	1250	Single pixel		
17/2/03	1750		1750	
	1800		1800	
	1810		1810	

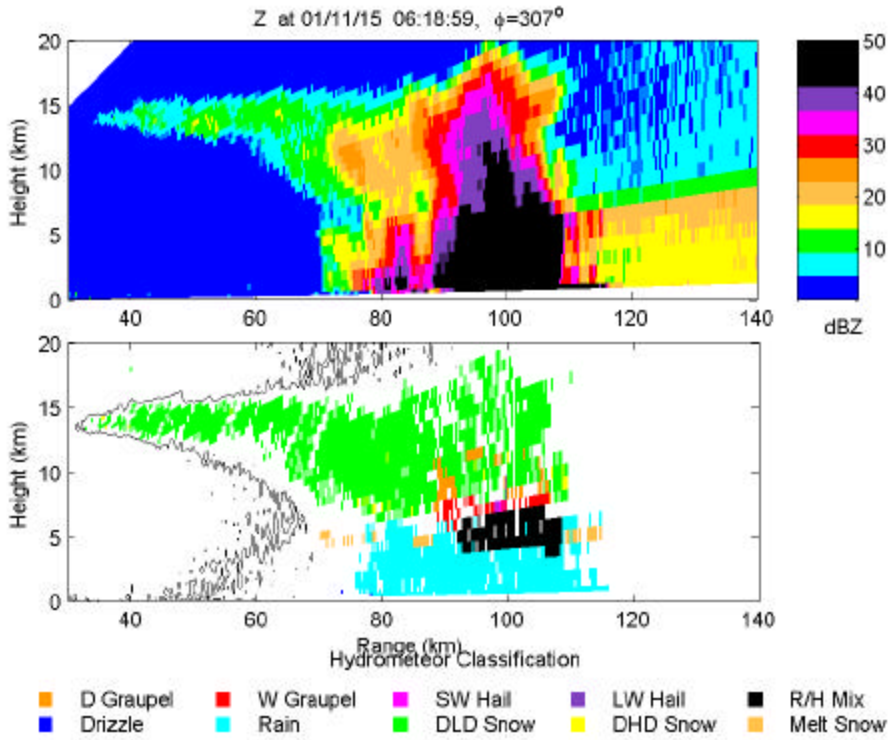

Figure 1 RHI cross-section of a thunderstorm over the Tiwi Islands north of Darwin. Note the flare echo extending behind the cell coinciding with the detection of a rain hail mixture.

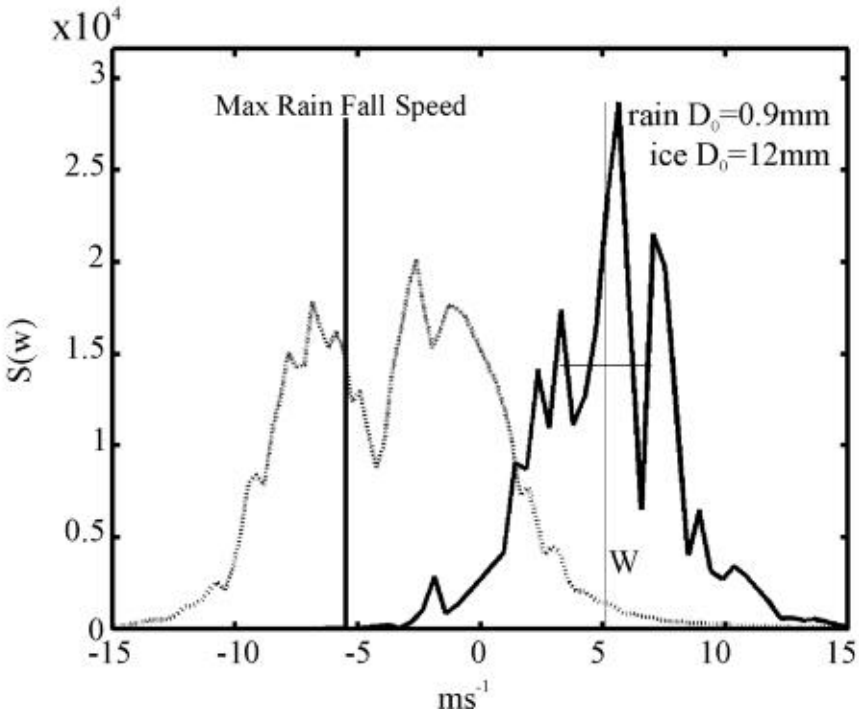

Figure 2 **Doppler spectra collected with the 50 Mhz profiler (solid) and 920 MHz profiler (dotted) at Darwin. The asymptotic limit for rain fall speeds relative to the mean air motion (w~ 5ms^{-1}) seen by the 50 MHz profiler is also included. The high fall speed peak corresponds to hail while the other is rain (After May et al., 2001)**

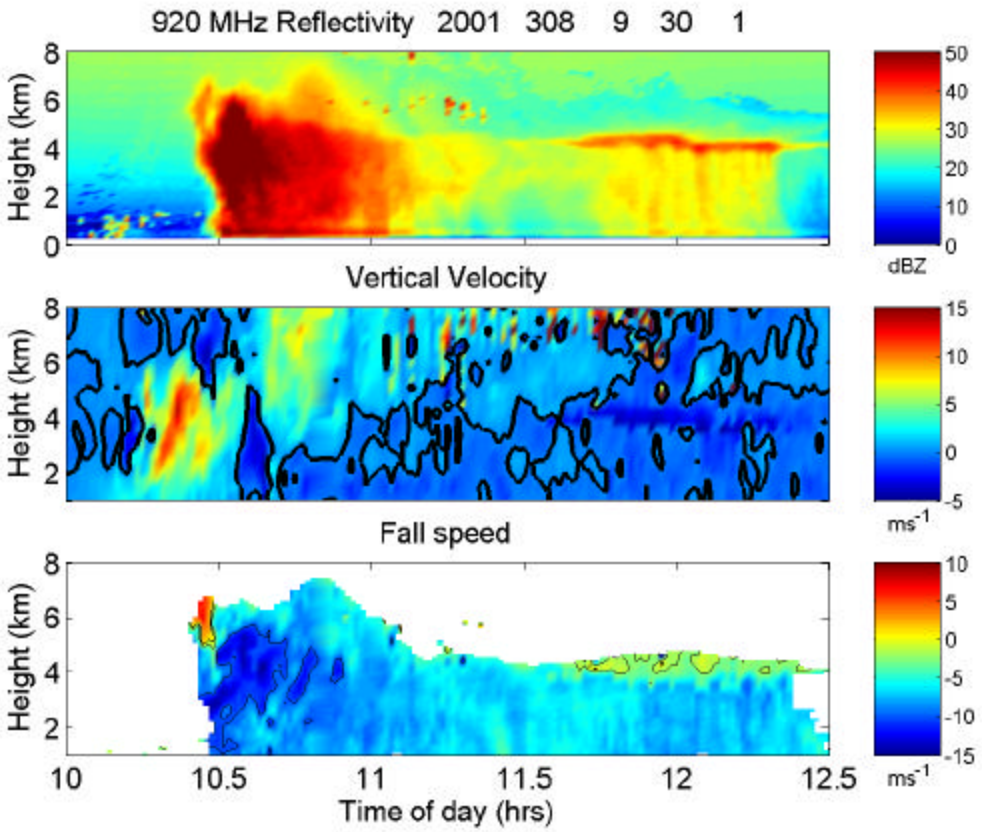

Figure 3 Time height cross-sections of the reflectivity measured with the 920 MHz profiler between 1000 and 1230 UTC on November 4, 2001 (top), mean vertical motion measured with the 50 MHz profiler with an overlaid contour of zero vertical motion (middle) and the reflectivity weighted precipitation fall speed estimated by the difference between the Doppler velocity measured with the 920 MHz profiler and the vertical motion subtracted. The contours of the lower panel are at fall speeds of -2 and -10 ms $^{-1}$.

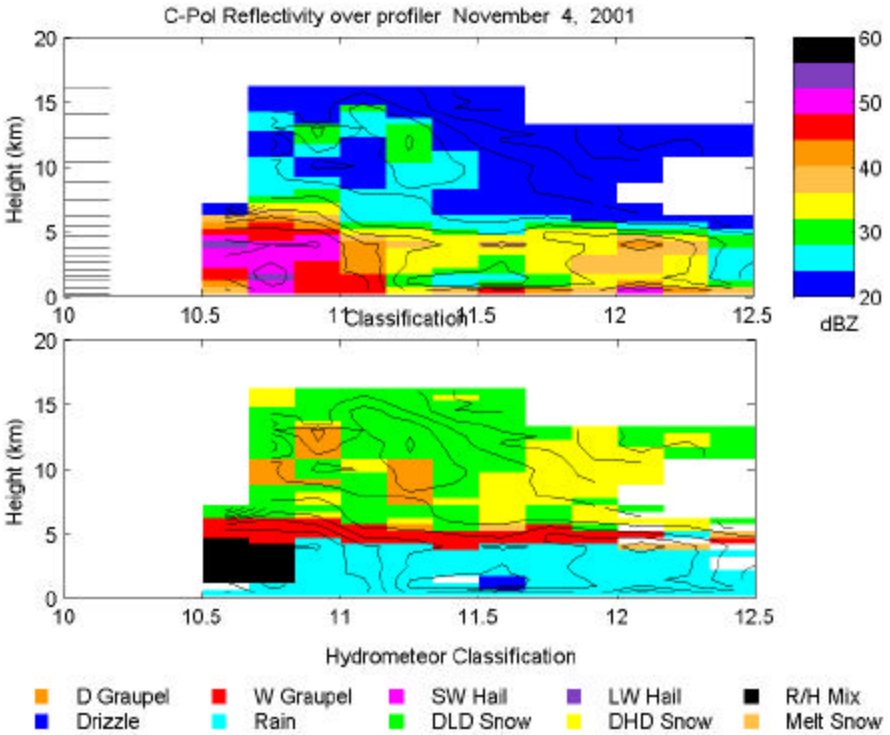

Figure 4 Time height cross-section of the C-Pol measurements of reflectivity on the grid point closest to the wind profiler location between 1000 and 1230 UTC on November 4, 2001 (top) and the corresponding microphysical classification. These data are on 2.5 by 2.5 km grids with a vertical sampling of 500m. The actual beam heights that were used in creating these data are marked by the horizontal lines on the left of the top panel.. Contours of reflectivity are overlaid on this figure.

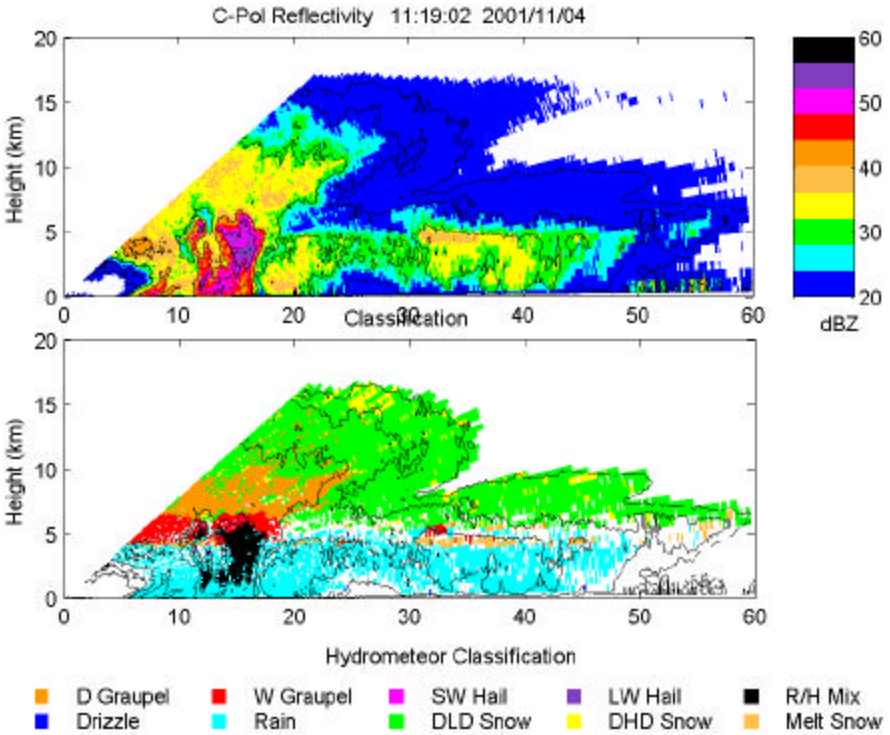

Figure 5 RHI scan at 1119 UTC on November 4, 2001 showing the reflectivity (top) and classification (bottom) . This shows an active convective element with a rain-hail mixture as well as a large area of wet graupel around the cell core. Of particular interest here is the narrow layer of melting snow that is resolved in the stratiform region farther from the radar. Contours of radar reflectivity are overlaid on these panels.

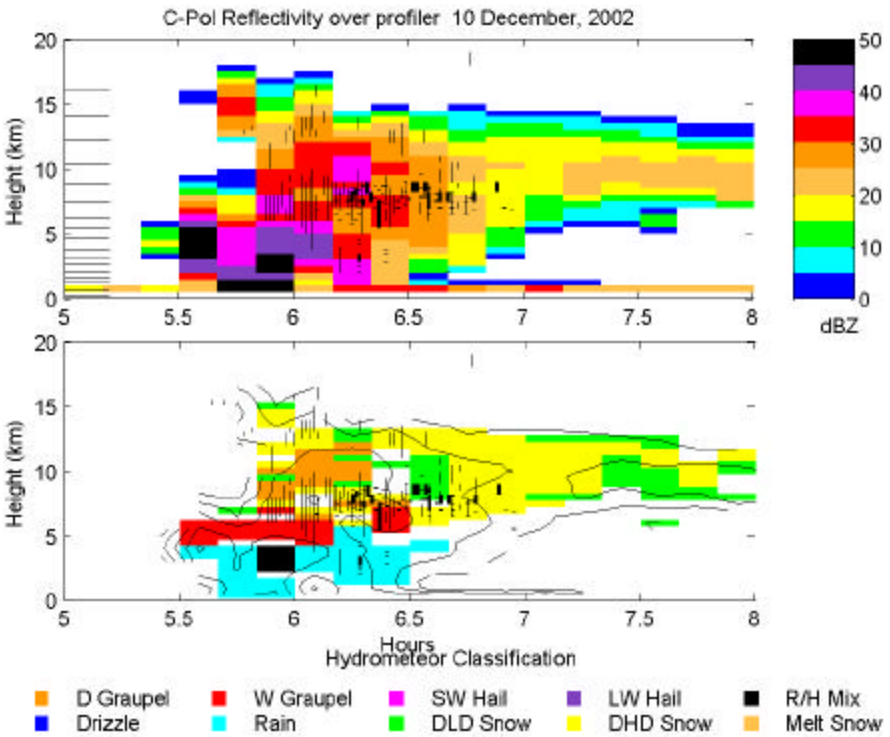

Figure 6 Another time height cross-section of the reflectivity and classifications for 0500 to 1000 UTC on December 10, 2002. However, in this case the location of lightning echoes in the profiler data have been overlayed (dark lines) along with contours of reflectivity as before. This was a very electrically active case although the most intense convection missed the profiler. However, an extensive region of wet graupel is visible prior to and in the electrically active period.